Simulation of Turbulent Lifted Flames and their Transient Propagation

S. Ruan, Z. Chen, N. Swaminathan
University of Cambridge
Cambridge, UK

1 Introduction

Turbulent lifted flame have been the subject of many studies [1,2] and its modelling is challenging. This is because the combustion model need to capture many different factors that contribute to the lifted flame stabilisation. These factors include premixed flame propagation [3], diffusion flamelet quenching [4], large scale flow structure [5], partial premixing and edge flame propagation [6]. Different modelling approaches have been used to compute the final lift-off height, including flamelet based modelling [7–11], Conditional Moment Closure [12, 13] and G-equation modelling approach [14, 15].

While the final lift-off height of turbulent lifted flames have been studied extensively in the past, their transient propagation characteristics from initial ignition to final stabilisation have only received very limited attention [11, 16, 17]. Ahmed and Mastorakos [16] performed experiment to measure the time history of a lifted methane flame propagation with two different inlet velocity cases. Lacaze et al. [17] computed one of this cases with Large Eddy Simulation (LES) with a thickened flame model. Chen et al. [11] performed simulations for all the cases with unsteady Reynolds Averaged Navier Stokes (RANS) with a flamelet model [10] that have included both premixed and non-premixed combustion contributions. Good final lift-off height and time history of lift-off height are obtained in comparison with experimental measurement. However, it remains to be tested that whether this model can capture the final lift-off height along with its temporal evolution of turbulent lifted flames with various fuels over a wide range of inlet velocity. This is a more challenging task as it requires the model to capture the various processes in turbulent flame from its initial ignition, development and propagation, to its final stabilisation. Furthermore, although analytical studies and empirical scaling [6, 18, 19] for the final lift-off height have been proposed in the past, scaling law for its temporal evolution has not been studied previously. This study attempts to compute and analyse the time series of the lift-off height data in order to understand the physical processes governing the various stages of the flame evolution til its stabilisation.

The objective of the current study is twofold. Firstly, to further test the combustion model for turbulent lifted flames of various fuels and over a wide range of inlet velocity and diameters. Secondly, to compute and analyse the transient flame propagation.

2 Combustion Modelling

The partially premixed flame (PPF) model developed in previous studies [10, 11] were used in this study. Only a brief summary of the model features are included here and details can be found in [10, 11]. The transport equations for the mixture fraction and the progress variable, their mean $\widetilde{Z}$ and $\widetilde{c}$, and variance $\widetilde{Z''^2}$, $\widetilde{c''^2}$ and $\widetilde{c''Z''}$ were solved along with the conservation equations for mass, momentum and energy. The transport equations for $\widetilde{c}$ and $\widetilde{c''Z''}$ need some attention and are given below.

$$\frac{\partial \overline{\rho}\widetilde{c}}{\partial t} + \frac{\partial \overline{\rho}\,\widetilde{u}_k\,\widetilde{c}}{\partial x_k} = \frac{\partial}{\partial x_k}\left(\overline{\rho D \frac{\partial c}{\partial x_k}} - \overline{\rho\, u_k'' c''}\right) + \overline{\dot{\omega}}_c^*, \tag{1}$$

where $\overline{\dot{\omega}_c^*}$ denotes the total reaction rate. Since the mixing and chemical reaction are strongly coupled in partially premixed combustion, one can not ignore their statistical correlation and thus the covariance $\widetilde{c''Z''}$ must also be included in the analysis. This equation is written as [10, 20]

$$\begin{aligned}\frac{\partial \overline{\rho}\,\widetilde{c''Z''}}{\partial t} + \frac{\partial \overline{\rho}\,\widetilde{u}_k\,\widetilde{c''Z''}}{\partial x_k} &= \frac{\partial}{\partial x_k}\left(\overline{\rho D \frac{\partial c'' Z''}{\partial x_k}} - \overline{\rho u_k'' c'' Z''}\right)\\ &\quad -2\,\overline{\rho}\,\widetilde{\epsilon}_{cZ} - \overline{\rho\, u_k'' c''}\frac{\partial \widetilde{Z}}{\partial x_k} - \overline{\rho\, u_k'' Z''}\frac{\partial \widetilde{c}}{\partial x_k} + \overline{Z''\dot{\omega}_c''^*}.\end{aligned} \tag{2}$$

The mean reaction rate, $\overline{\dot{\omega}_c^*}$, in the transport equation for c can be written as [21]

$$\overline{\dot{\omega}_c^*} = \overline{\frac{1}{\partial\psi/\partial c}\left(\dot{\omega}_\psi + 2\rho N_{cZ}\frac{\partial^2\psi}{\partial c\partial Z} + \rho N_{ZZ}\frac{\partial^2\psi}{\partial Z^2} + \rho N_{cc}\frac{\partial^2\psi}{\partial c^2}\right)}, \tag{3}$$

where $\dot{\omega}_\psi$ is the reaction rate for ψ. The three instantaneous scalar dissipation rates are defined as $N_{ZZ} = D(\nabla Z\cdot\nabla Z)$, $N_{Zc} = D(\nabla c\cdot\nabla Z)$ and $N_{cc} = D(\nabla c\cdot\nabla c)$.

It was shown [10] that Eq.(3) can be reduced to

$$\overline{\dot{\omega}_c^*} = \overline{\dot{\omega}}_c + \underbrace{\overline{\rho N_{ZZ}\frac{c}{\psi^{Eq}}\frac{d^2\psi^{Eq}}{dZ^2}}}_{\overline{\dot{\omega}}_{\rm np}} + \underbrace{\overline{2\rho N_{Zc}\frac{1}{\psi^{Eq}}\frac{d\psi^{Eq}}{dZ}}}_{\overline{\dot{\omega}}_{\rm cdr}}. \tag{4}$$

The first part signifies the contribution of premixed mode combustion, the second part, $\overline{\dot{\omega}}_{\rm np}$, signifies the contributions from non-premixed mode and the third part, $\overline{\dot{\omega}}_{\rm cdr}$, denotes a contribution resulting from interactions of Z and c gradients. Previous studies [22] showed that the cross dissipation contribution is an order of magnitude smaller than the contributions from the other two terms and thus $\overline{\dot{\omega}}_{\rm cdr}$ is neglected from further consideration in this work. The other two terms are modelled as follows.

The first term of Eq. (4) is modelled as [10]

$$\overline{\dot{\omega}}_c = \overline{\rho}\int_0^1\int_0^1\left[\frac{\dot{\omega}_c(\zeta,\xi)}{\rho(\zeta,\xi)}\right]\widetilde{P}(\zeta,\xi)\quad d\zeta\, d\xi, \tag{5}$$

where $\overline{\rho}$ is the mean local mixture density obtained as described in the later part of this subsection. The flamelet reaction rate, $\dot{\omega}_c(\zeta,\xi)$, and mixture density, $\rho(\zeta,\xi)$, are obtained from laminar unstrained premixed flame calculation. The Favre joint PDF, $\widetilde{P}(\zeta,\xi)$, including Z-c correlation is calculated using the copula method described in [10]. This correlation is calculated using the covariance, $\widetilde{c''Z''}$, obtained from its transport equations, Eq. (2).

The second term, $\overline{\dot{\omega}}_{\rm np}$, denoting contributions of non-premixed mode combustion is modelled as [10]

$$\overline{\dot{\omega}}_{\rm np} \simeq \overline{\rho}\,\widetilde{c}\,\widetilde{\epsilon}_{ZZ}\int_0^1 \frac{1}{\psi^{Eq}(\xi)}\frac{d^2\psi^{Eq}(\xi)}{dZ^2}\,\widetilde{P}_\beta(\xi)\quad d\xi. \tag{6}$$

Further modelling details can be found in [10, 11].

3 Experimental Test Cases

The experiments of turbulent lifted flames of hydrogen [23, 24], methane [16, 18, 25, 26] and propane [18] have been used as test cases. The range of inlet velocity are 300-900 m/s for hydrogen flames, 20-105 m/s for methane flames, 30-75 m/s for propane flames. The inlet nozzles diameters are 2mm for hydrogen flames, 4mm, 5mm and 8mm for methane flames, and 6.1mm for propane flames. This is an extensive collection of experimental measurement for turbulent lifted flames with a wide range of conditions, including inlet diameter, velocity and fuels. Some of these flames have been studied previously [10, 11]. A total of 26 test cases were computed using the PPF model here.

4 Numerical Setup

The PPF model noted earlier has been implemented in a commercial CFD code FLUENT. User defined functions (UDFs) were used to include extra transport equations for $\widetilde{Z}$, $\widetilde{c}$, $\widetilde{Z''^2}$, $\widetilde{c''^2}$, $\widetilde{c''Z''}$ and $\widetilde{h}$. 2-D axisymmetric unstructured grids were used. A total of five different grids were used to tailor the different test cases. They are refined along the jet shear layers. Each grid has been carefully tested to ensure the final lift-off height results were not sensitive to the grid. The k-ϵ turbulence model was used where the model constant were adjusted according to previous studies [10, 11] to give a better flow field description. Further details of numerical setup can be found in [10, 11].

5 Results and Discussion

Figure 1 presents the comparison of computed lift-off height with PPF model and the experimental measurements for CH4, H2 and C3H8 flames with different inlet diameters and velocities. Note that Fig.1(b) was shown in earlier study [10]. In general, the PPF model gives very good lift-off height results compared to the experiments in all conditions.

Figure 2 shows the computed temporal evolution of the flame brush for the hydrogen lifted flame with inlet velocity of 680 m/s. The time has been normalised by the flow time using nozzle diameter and inlet velocity $t^* = t/(D/U)$. The stoichiometric mixture fraction isoline, the rich and lean limit of mixture fraction isolines are also shown in the figure. As the flame was ignited at the stoichiometric mixture with a flame kernel initialised, it quickly grew in size and divided into two parts, one propagated upstream and the other moved downstream along the stoichiometric mixture isoline. The part propagating upstream soon formed two distinct branches, one lean and one rich. While the lean flame branch can be observed close to the lean limit, the rich branch was further away from the rich limit, as the rich mixture close to the jet centre experienced a very high mean velocity that made the rich branch flame propagation more difficult. This observation of various stages from flame ignition to its final stabilisation for H2 flame is qualitatively similar to earlier study [11] for CH4 flames.

Before moving on to quantitative analysis the computed transient characteristic of flame evolution from initial ignition to its final stabilisation, we like to establish the validity of our unsteady simulation for the temporal evolution of flame lift-off height by comparing the computed time series with experimental measurement. Figure 3 compares the temporal evolution of lift-off height obtained from PPF model and experimental measurement [16]. The time series of lift-off height is for a CH4 flame with 30% air dilution with inlet velocity of 12.5 m/s. Both time series for flame igition position at 30D and 40D are shown. Note that this figure was shown in [11] and is included here for completeness. It is observed that the computed results are good for the case where igition was at 30D. For the 40D case, the computed results are reasonable but over-estmate the speed of flame propagation . As discussed previously [11], the difference in simulation and experiment can be due to the small sample size (only 10) during the

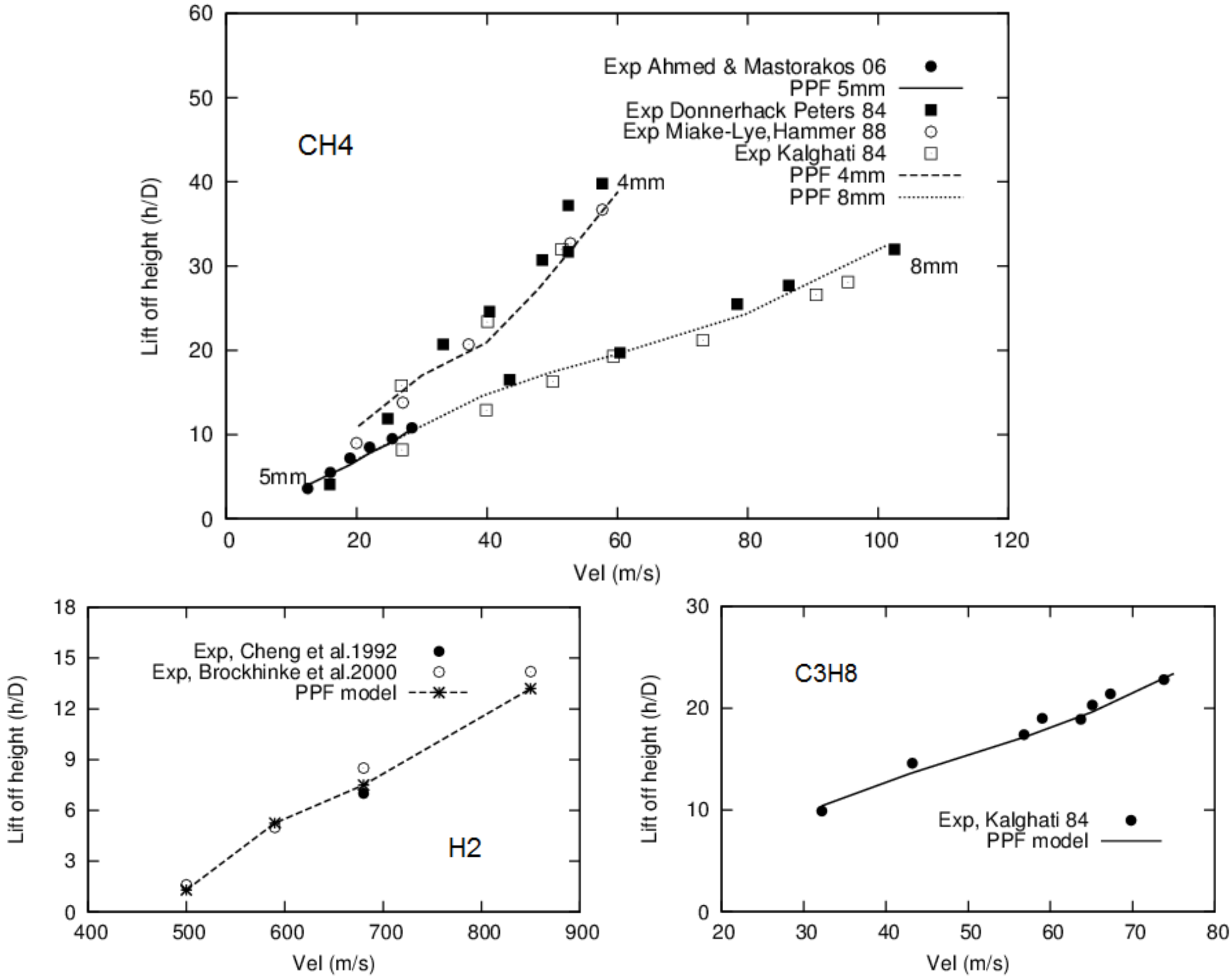

Figure 1: Lift-off height against inlet velocity for (a) CH4 flames with inlet diameter of 4mm, 5mm and 8mm. (b) H2 flames with inlet diameter of 2mm. (c) C3H8 flames with inlet diameter of 6mm.

experiment, and also that the role of large flow structure may not be adequately captured by the current two dimensional RANS simulation. Nevertheless, the comparison is reasonable and gives us confidence in analysing the computed time series for the H2 and C3H8 flames where experimental measurement of time history of lift-off height is not available.

Figure 4 presents the temporal evolution of lift-off height for the H2 flames with inlet velocity of 680 m/s for two cases. The flames were ignited at about the same axial position (11.5D-11.75D) but different radial positions. Therefore, at ignition positions, the local mean mixture fraction are 0.03 and 0.075, and the mean velocity are 65 m/s and 95 m/s for case A and B respectively. It is therefore not surprising to see the flame kernel initialised in a weaker mixture and higher velocity was being convected downstream before it propagated upstream again, and it took longer time to reach its stabilisation height, as shown in Fig.4. It is clear the flame firstly propagates in a higher speed during the earlier stage to about $t^* = 300$ then slowed down to another speed at the next stage until it finally stabilised. A closer examination (not shown here) of the flow field ahead of the flame leading edge shows a short period of reverse flow which coincides with the early flame propagation stage. This reverse flow aided the flame propagation. Further analysis of the flow and flame data is necessary to shed light on its transient flame propagation behaviour and attempt to propose scaling law governing the temporal flame evolution.

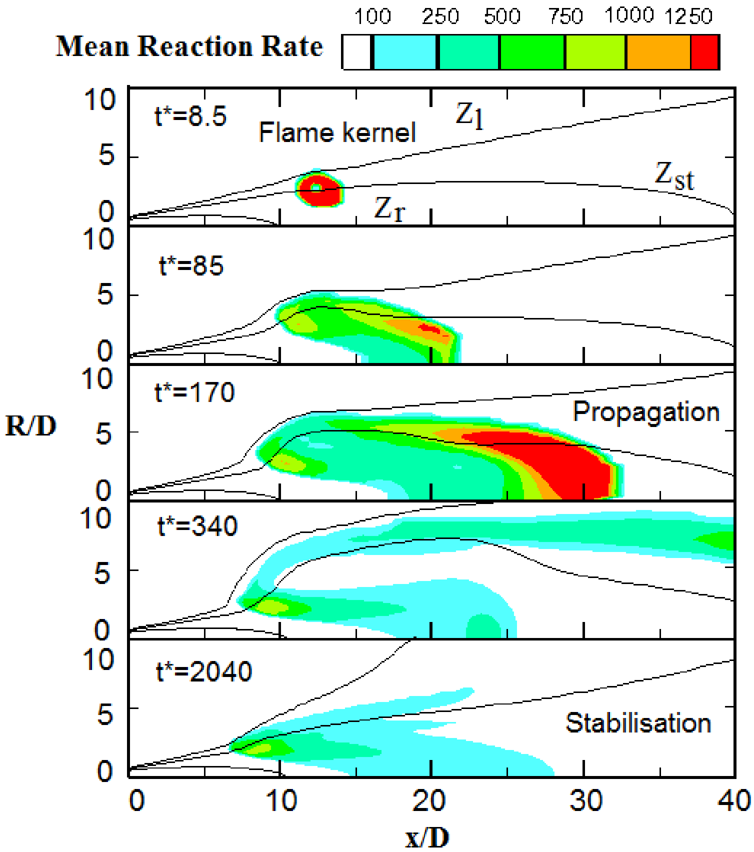

Figure 2: The computed flame brush evolution for H2 flames of 680 m/s.

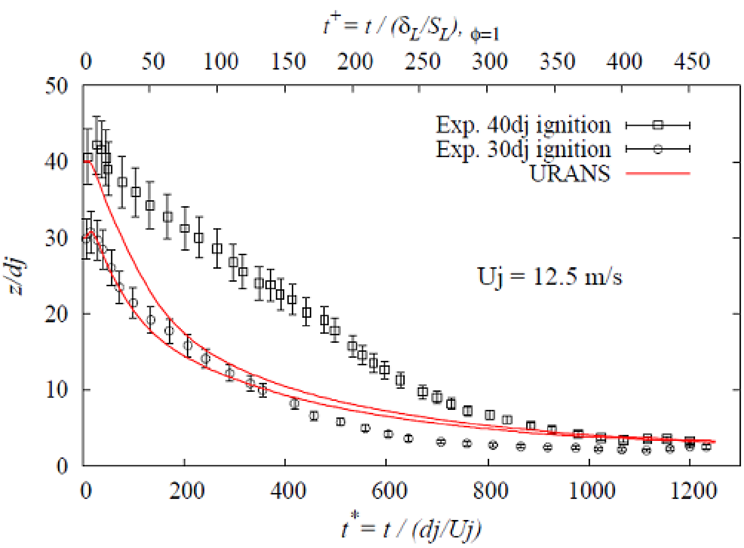

Figure 3: Comparison of temporal evolution of lift-off height for CH4 flames with 30% air dilution from PPF model and experimental measurement. Flames were ignited at 30D and 40D. Inlet velocity is 12.5 m/s.

References

[1] W. M. Pitts, Proc. Combust. Inst. 22 (1988) 809–816.

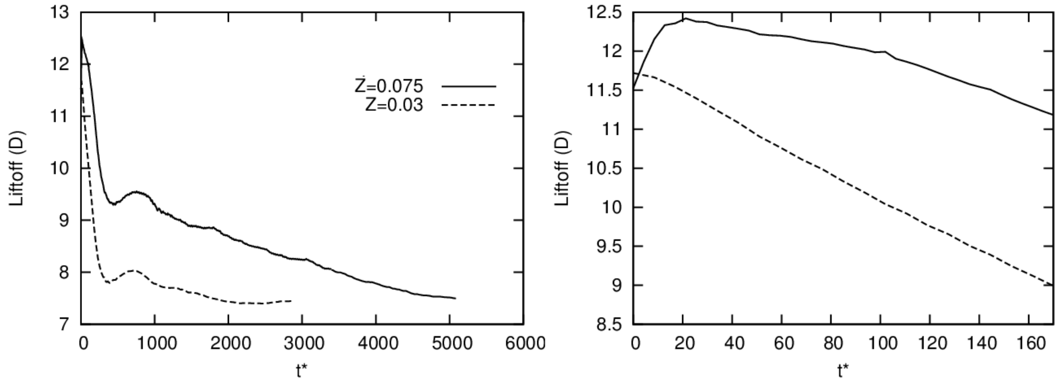

Figure 4: Comparison of temporal evolution of lift-off height for H2 flames obtained from PPF model for different ignition positions. (Enlarged view at the right.)

[2] K. M. Lyons, Prog. Energy Combust. Sci. 33 (2007) 211–231.

[3] L. Vanquickenborne, A. van Tiggenlen, Combust. Sci. Technol. 10 (1966) 59–69.

[4] N. Peters, F. A. Williams, AIAA J. 21 (1983) 423–429.

[5] J. E. Broadwell, W. J. A. Dahm, M. G. Mungal, Proc. Combust. Inst. 20 (1984) 303–310.

[6] A. Upatnieks, J. F. Driscoll, C. C. Rasmussen, S. L. Ceccio, Combust. Flame 138 (2004) 259–272.

[7] D. Bradley, P. Gaskell, A. Lau, Symposium (International) on Combustion 23 (1) (1991) 685 – 692.

[8] D. Bradley, P. Gaskell, X. Gu, Symposium (International) on Combustion 27 (1) (1998) 1199 – 1206.

[9] L. Vervisch, R. Hauguel, P. Domingo, M. Rullaud, J. Turbulence 5 (2004) 004.

[10] S. Ruan, N. Swaminathan, O. Darbyshire, Combust. Theory Model. 18 (2014) 295–329.

[11] Z. Chen, S. Ruan, N. Swaminathan, Combustion and Flame.

[12] C. Devaud, K. N. C. . Bray, Combust. Flame 132 (2003) 102–114.

[13] I. Kim, E. Mastorakos, Proc. Combust. Inst. 30 (2005) 911–918.

[14] C. M. Müller, H. Breitbach, N. Peters, Proc. Combust. Inst. 25 (1994) 1099–1106.

[15] M. Chen, M. Herrmann, N. Peters, Proc. Combust. Inst. 28 (2000) 167–174.

[16] S. Ahmed, E. Mastorakos, Combustion and Flame 146 (1–2) (2006) 215 – 231.

[17] G. Lacaze, E. Richardson, T. Poinsot, Combustion and Flame 156 (10) (2009) 1993 – 2009.

[18] G. Kalghatgi, Combustion Science and Technology 41 (1-2) (1984) 17–29.

[19] H. Eickhoff, Combust. Flame 142 (2005) 324–325.

[20] O. Darbyshire, N. Swaminathan, Combust. Sci. Technol. 184 (2012) 2036–2067.

[21] K. N. C. Bray, P. Domingo, L. Vervisch, Combust. Flame 141 (2005) 431–437.

[22] S. Ruan, N. Swaminathan, K. N. C. Bray, Y. Mizobuchi, T. Takeno, Combust. Flame 159 (2012) 591–608.

[23] T. Cheng, J. A. Wehrmeyer, R. W. Pitz, Combust. Flame 91 (1992) 323–345.

[24] A. Brockhinke, S. Haufe, K. Kohse-hoinghaus, Combust. Flame 121 (2000) 367–377.

[25] R. C. Miake-Lye, J. A. Hammer, Proc. Combust. Inst. 22 (1989) 817–824.

[26] S. Donnerhack, N. Peters, Combust. Sci. Technol. 41 (1984) 101–108.